AGU PUBLICATIONS

Paleoceanography

RESEARCH ARTICLE
10.1002/2017PA003166

Key Points:
- Late Pliocene marine and terrestrial climate in the Norwegian Sea region is controlled by Norwegian Atlantic Current and obliquity changes
- Warmer-than-present intervals characterized by strong Norwegian Atlantic Current influence and high obliquity
- During colder late Pliocene intervals, oceanic and terrestrial conditions were comparable to the present

Supporting Information:
- Supporting Information S1
- Data Set S1

Correspondence to:
S. Panitz,
sina.panitz@gmail.com

Citation:
Panitz, S., De Schepper, S., Salzmann, U., Bachem, P. E., Risebrobakken, B., Clotten, C., & Hocking, E. P. (2017). Mid-Piacenzian variability of Nordic Seas surface circulation linked to terrestrial climatic change in Norway. *Paleoceanography*, *32*, 1336–1351. https://doi.org/10.1002/2017PA003166

Received 25 MAY 2017
Accepted 6 NOV 2017
Accepted article online 9 NOV 2017
Published online 4 DEC 2017

Mid-Piacenzian Variability of Nordic Seas Surface Circulation Linked to Terrestrial Climatic Change in Norway

Sina Panitz[1], Stijn De Schepper[2], Ulrich Salzmann[1], Paul E. Bachem[2], Bjørg Risebrobakken[2], Caroline Clotten[2], and Emma P. Hocking[1]

[1]Department of Geography, Faculty of Engineering and Environment, Northumbria University, Newcastle upon Tyne, UK, [2]Uni Research Climate, Bjerknes Centre for Climate Research, Bergen, Norway

Abstract During the mid-Piacenzian, Nordic Seas sea surface temperatures (SSTs) were higher than today. While SSTs provide crucial climatic information, on their own they do not allow a reconstruction of potential underlying changes in water masses and currents. A new dinoflagellate cyst record for Ocean Drilling Program (ODP) Site 642 is presented to evaluate changes in northward heat transport via the Norwegian Atlantic Current (NwAC) between 3.320 and 3.137 Ma. The record is compared with vegetation and SST reconstructions from Site 642 and SSTs from Iceland Sea ODP Site 907 to identify links between SSTs, ocean currents, and vegetation changes. The dinocyst record shows that strong Atlantic water influence via the NwAC corresponds to higher-than-present SSTs and cool temperate vegetation during Marine Isotope Stage (MIS) transition M2–M1 and KM5. Reduced Atlantic water inflow relative to the warm stages coincides with near-modern SSTs and boreal vegetation during MIS M2, KM6, and KM4–KM2. During most of the studied interval, a strong SST gradient between Sites 642 and 907 indicates the presence of a proto-Arctic Front (AF). An absent gradient during the first half of MIS KM6, due to reduced Atlantic water influence at Site 642 and warm, presumably Atlantic water reaching Site 907, is indicative of a weakened NwAC and East Greenland Current. We conclude that repeated changes in Atlantic water influence directly affect terrestrial climate and that an active NwAC is needed for an AF to develop. Obliquity forcing may have played a role, but the correlation is not consistent.

Plain Language Summary At present, northward heat transport via the Norwegian Atlantic Current (NwAC) is a major reason for the mild climate in Norway. For the warmer-than-present late Pliocene (approximately 3.0–3.3 Ma), it is unclear if changes in northward heat transport affected the Norwegian Sea and Scandinavian climate. We analyzed fossil dinoflagellate cysts in Ocean Drilling Program Hole 642B to reconstruct changes in the influence of the NwAC during the late Pliocene. We found that strong NwAC influence and changes in insolation are responsible for warmer-than-present climatic conditions in Norway. In contrast, reduced NwAC influence is associated with similar-to-present climatic conditions on land. These results highlight that changes in northward heat transport via the NwAC and insolation changes control late Pliocene climate changes in Norway.

1. Introduction

The mid-Piacenzian (3.264–3.025 Ma) is the most recent prolonged warm period in Earth's history that exhibits similarities to climatic conditions predicted for the end of the 21st century (Dowsett et al., 2016; Intergovernmental Panel on Climate Change, 2013). As such, this time interval has been the focus of proxy reconstructions and climate modeling to compile a comprehensive picture of the magnitude and spatial scale of climatic changes and their drivers (Dowsett et al., 2016; Haywood et al., 2016). During the mid-Piacenzian, global annual surface temperatures are estimated to have been 2–3°C higher than present, with reconstructed atmospheric CO_2 concentrations ranging between 270 and 410 ppm (Badger et al., 2013; Bartoli et al., 2011; Haywood, Hill, et al., 2013; Martínez-Botí et al., 2015; Seki et al., 2010). The most recent environmental reconstruction of this time interval, the Pliocene Research Interpretation and Synoptic Mapping (PRISM) 4 paleoenvironmental reconstruction, highlights the need for high-resolution multiproxy records with a regional and process-oriented approach (Dowsett et al., 2016; Dowsett, Robinson, et al., 2013). Such studies are needed to provide more complete paleoenvironmental reconstructions and to gain a better understanding of the climate variability within the mid-Piacenzian (McClymont et al., 2015). Furthermore, there is significant disagreement between data and models over the magnitude of warming

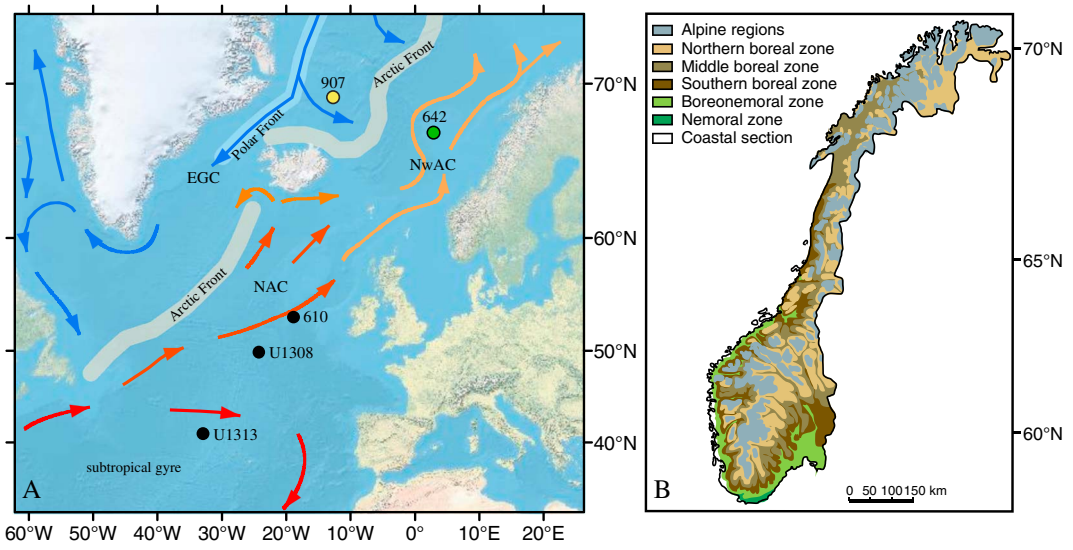

Figure 1. Modern oceanographic setting and vegetation of Norway. Location of (a) Ocean Drilling Program (ODP) Site 642 in the Norwegian Sea (green circle, this study), Site 907 (yellow circle, this study) in the Iceland Sea, Deep Sea Drilling Project Site (DSDP) 610, and Integrated Ocean Drilling Program (IODP) sites U1308 and U1313 in the North Atlantic (black circles). (b) Modern vegetation of Norway modified after Moen (1987). In Figure 1a, color gradient of currents from red to light orange indicates decreasing water temperatures and blue designates cold currents. EGC = East Greenland Current, NAC = North Atlantic Current, and NwAC = Norwegian Atlantic Current.

during the mid-Piacenzian, highlighting the need for further investigations (Dowsett, Foley, et al., 2013; Haywood, Dolan, et al., 2013; Salzmann et al., 2013).

In the Nordic Seas, some proxy-based reconstructions reveal an enhanced sea surface temperature (SST) increase when compared to low-latitude sites during the mid-Piacenzian (Dowsett, Foley, et al., 2013). This has been ascribed to increased northward heat transport via a stronger Atlantic Meridional Overturning Circulation (Ravelo & Andreasen, 2000; Raymo et al., 1996; Sarnthein et al., 2009), radiative forcing due to increased greenhouse gas levels (Bachem et al., 2016; Zhang, Nisancioglu, Chandler, et al., 2013; Zhang, Nisancioglu, & Ninnemann, 2013), and paleogeographic changes in the Arctic (Hill, 2015; Otto-Bliesner et al., 2017). In fact, the magnitude of warming is not uniform over the Nordic Seas and varies between proxies and sites. At Ocean Drilling Program (ODP) Site 907 (69°N) in the Iceland Sea (Figure 1), the reconstruction of summer SSTs using the Mg/Ca ratio yields values 3–5°C higher than present (Robinson, 2009), and an estimate of annual SSTs derived from alkenones at the same site is around 3°C higher than today (Schreck et al., 2013). At ODP Site 909 (79°N) northwest of Svalbard, summer SSTs using alkenones and the Mg/Ca ratio have been estimated to be ~11–18°C higher than present (Robinson, 2009). However, the full variability may not be recorded due to low resolution of the data sets and the estimates might only represent brief pulses of warmth advecting into the Arctic (Robinson, 2009). At the nearby Site 910 (80°N), a rise of annual SSTs of 3–4°C is inferred from the distribution of glycerol dialkyl glycerol tetraethers (Knies, Cabedo-Sanz, et al., 2014). The warming is least pronounced in the Norwegian Sea. There, alkenone-derived summer SST estimates for the mid-Piacenzian show a warming in the order of 2–3°C in comparison to the Holocene average, with an obliquity-driven SST variability of up to 4°C (Bachem et al., 2016). Bachem et al. (2016) suggest that the inflow of warm Atlantic water into the Norwegian Sea via the North Atlantic Current (NAC) was similar to present. However, these estimates are only based on SST reconstructions and the large variety in reconstructed temperatures between sites emphasizes the need for better documentation of the mid-Piacenzian oceanographic conditions and climate variability in the Nordic Seas.

In the North Atlantic, variations in strength and position of the NAC recorded in dinoflagellate cyst (dinocyst) and SST records have been suggested to have had a strong impact on high-latitude climate during glacial Marine Isotope Stage (MIS) M2 (approximately 3.3 Ma) and the subsequent establishment of warmer climatic conditions during the mid-Piacenzian (De Schepper et al., 2013). A weakened NAC appears to have halted northward heat transport prior to the global ice volume expansion during MIS M2, whereas the

reestablishment of an active, modern-like NAC corresponds to the onset of mid-Piacenzian warm conditions (De Schepper et al., 2013). In northern Norway, the continuous presence of cool temperate and boreal forests on land indicates that mid-Piacenzian climate was too warm for the persistence of sea-terminating glaciers, even during MIS M2 (Panitz et al., 2016). It remains unclear whether the Scandinavian terrestrial realm and Nordic Seas SST changes are linked to variations in the inflow of Atlantic water into the Norwegian Sea or can merely be explained by orbitally forced insolation changes. In particular, evidence for changes in the inflow of Atlantic water and its effects on terrestrial climate is missing for the Norwegian Sea—a region crucial for heat transport from the North Atlantic to the Arctic Ocean via the Norwegian Atlantic Current (NwAC).

Here we integrate a new high-resolution dinoflagellate cyst record from ODP Hole 642B in the Norwegian Sea with pollen (Panitz et al., 2016), alkenone-derived SSTs, and ice rafted debris (IRD) records from the same site (Bachem et al., 2017) over a ~180 kyrs time interval (3.320–3.137 Ma). This multiproxy approach allows us to document surface water mass changes in the Norwegian Sea throughout the mid-Piacenzian and investigate land-ocean interactions, as well as oceanographic and atmospheric forcings. ODP Site 642 represents one of two PRISM4 time series in the North Atlantic region that allow a comparison of marine and terrestrial environmental changes during the mid-Piacenzian (Dowsett et al., 2016).

2. Geographical Setting

The Nordic Seas consist of the Greenland Sea, Iceland Sea, and Norwegian Sea and are characterized by steep zonal and meridional climatic gradients. ODP Site 642 is located on the outer Vøring Plateau in the Norwegian Sea, about 400–450 km west off the Norwegian coast (67°13.2′N, 2°55.8′E, 1,286 m water depth; Shipboard Scientific Party, 1987; Figure 1). The site is situated in the path of the northward flowing NwAC, with one branch on either side of the plateau. The eastern branch follows the Norwegian continental slope and the western branch flows around the Vøring Plateau (Nilsen & Nilsen, 2007). The NwAC is a continuation of the NAC, with Atlantic waters entering the Norwegian Sea through the Iceland-Faroe Ridge and Faroe-Shetland Channel, resulting in the presence of warm and saline (6–10°C, 35.1–35.3 practical salinity unit, psu, in summer) waters (Blindheim & Østerhus, 2005; Swift, 1986). The warm, nutrient-enriched waters of the NAC are associated with relatively high primary production in the Norwegian Sea (Skogen et al., 2007). The NwAC gradually releases its excess heat along its way toward the Arctic Ocean. In the eastern Nordic Seas, cooler and fresher polar water from the Arctic (<0°C, 30–34 psu in summer) is transported southward within the East Greenland Current (EGC) (Swift, 1986). Along its path, some of the EGC water is diverted to the east into the adjacent Boreas Basin, Greenland Basin, and Iceland Sea (Blindheim & Østerhus, 2005). Polar and Atlantic water masses mix in the central part of the Nordic Seas, forming a distinct Arctic water mass (0–4°C, 34.6–34.9 psu in summer) (Swift, 1986). The water masses are separated by fronts, with the Polar Front following the southward flowing EGC, separating Polar and Arctic water, and the Arctic Front (AF), marking the boundary between Arctic and Atlantic water and running from SW to NE north of Iceland (Figure 1) (Swift, 1986).

Climate and vegetation of Norway change along latitudinal and altitudinal gradients as well as with increasing continentality. Due to the presence of Atlantic water, the climate of Norway is relatively mild when compared with areas at comparable latitudes (Diekmann, 1994). The modern vegetation of Norway is characterized by boreal forests, with alpine tundra prevailing at the higher altitudes of the Scandinavian mountains (Figure 1). Deciduous forest is found at the far southern coast of Norway (Figure 1) (Moen, 1987, 1999).

3. Materials and Methods

3.1. Age Model

The Pliocene age model for ODP Hole 642B is based on an updated magnetic stratigraphy (Bleil, 1989; Hilgen et al., 2012) and the correlation of the benthic oxygen isotope curve from Hole 642B to the global LR04 benthic oxygen isotope stack between 4.147 and 3.137 Ma (Figure 2) (Lisiecki & Raymo, 2005; Risebrobakken et al., 2016). A hiatus is present in the younger part (<3.14 Ma) of the Pliocene section (Jansen & Sjøholm, 1991). All records presented from Hole 642B follow the same age model (Risebrobakken et al., 2016).

3.2. Samples and Sample Preparation

Marine palynomorphs (dinocysts and acritarchs) were analyzed in 44 samples from ODP Hole 642B between 68.45 and 66.95 m below seafloor, or 3.32 and 3.14 Ma (Risebrobakken et al., 2016; Shipboard Scientific Party, 1987),

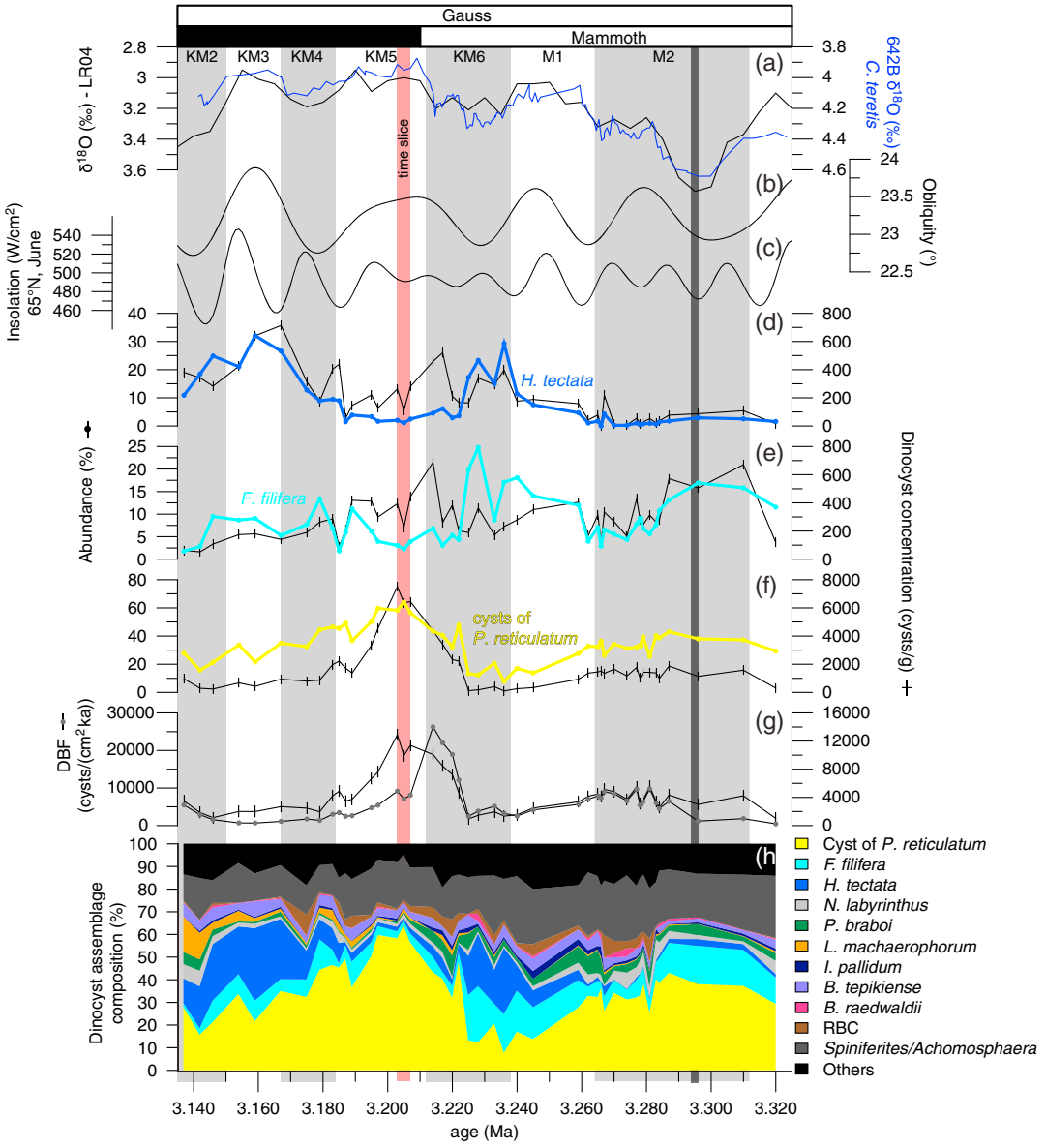

Figure 2. Dinoflagellate cyst (dinocyst) assemblages from ODP Hole 642B in the Norwegian Sea. (a) Global benthic oxygen isotope stack from Lisiecki and Raymo (2005) and the 5-point smoothed benthic oxygen isotope curve for Hole 642B from Risebrobakken et al. (2016); (b, c) orbital solutions for mean daily insolation and obliquity from Laskar et al. (2004); (d, f) relative abundance (colored lines) and concentration (black lines) of the dinocyst species *H. tectata*, *F. filifera*, and cysts of *P. reticulatum*; (g) dinocyst burial flux (DBF, line with gray dots) and total dinocyst concentration (line with vertical bars); and (h) Dinocyst assemblage composition in Hole 642B. Dark gray vertical bar indicates the possible presence of an hiatus over the most extreme part of marine isotope stage M2 (Risebrobakken et al., 2016). Light red bar marks KM5c the time slice chosen for data-model comparison (Haywood, Dolan, et al., 2013).

with three samples taken from De Schepper et al. (2015). The <63 μm sediment fraction was used for palynomorph analysis as the samples were presieved in Bergen, Norway, to retain foraminifera for oxygen isotope analysis (Risebrobakken et al., 2016). The samples were prepared at the Palynological Laboratory Services Ltd, North Wales, and Northumbria University, Newcastle, using standard palynological techniques (details in De Schepper et al., 2017). One *Lycopodium clavatum* spore tablet was added to each sample to calculate pollen concentrations (Stockmarr, 1971). The sediment was treated with HCl (20%) followed by concentrated HF (48%) to remove carbonates and silicates, respectively. Fluorosilicates were removed with an additional wash of hot (approximately 80°C) HCl (20%). The sediment was sieved through a 10 μm screen, and the back-sieved residue was mounted on glass slides using glycerol-gelatin jelly.

Marine [this study] and terrestrial (Panitz et al., 2016) palynomorphs were studied in the same samples, with both records having a temporal resolution of 1,000 to 14,000 years. Alkenone-derived SSTs from Hole 642B have been estimated in 87 samples between 3.138 and 3.330 Ma (Bachem et al., 2016, 2017). For six of the 44 samples analyzed for palynomorphs, SSTs are available from exactly the same sample.

Alkenone-derived SSTs from ODP Hole 907A (Figure 1) were obtained using the method described in Schreck et al. (2017). The age model for Hole 907A is based on Jansen et al. (2000). The raw data are available at https://doi.pangaea.de/10.1594/PANGAEA.877309.

3.3. Analysis of Marine Palynomorphs

3.3.1. Dinoflagellate Cysts

At least 300 dinocysts were identified for each sample, and Table 1 provides a taxonomic list of species encountered in the Piacenzian sediments of ODP Hole 642B. Cysts of *Protoceratium reticulatum* (also known as *Operculodinium centrocarpum* sensu Wall & Dale, 1966; see Paez-Reyes & Head, 2013) with processes smaller than 2 μm (cf. Rochon et al., 1999) were counted separately in 34 samples (the morphotype was not differentiated in the remaining 10 samples). *Brigantedinium* spp. comprises all (sub)spherical brown protoperidinioid cysts with an intercalary (sub)polygonal archeopyle and without processes (Reid, 1977). Round brown cysts (RBCs) include (sub)spherical brown protoperidinioid cysts with neither processes nor a visible polygonal archeopyle. Round brown spiny dinocysts without a visible archeopyle are included in *Echinidium* spp. Species within the genus *Spiniferites* were differentiated if possible, depending on orientation and preservation. The relative abundance of taxa was described as dominant (>60%), abundant (60–30%), common (30–10%), rare (10–1%), or present (1–0%).

The dinocyst burial flux (DBF) was calculated based on the dinocyst concentrations using the following formula:

$$\mathrm{DBF} = C_D \times \rho \times S \quad (1)$$

with DBF in cysts/(cm^2 ka). C_D is the dinocyst concentration (cysts/g), ρ the dry bulk density (g/cm^3) (Shipboard Scientific Party, 1987), and S the sedimentation rate (cm/ka) (Risebrobakken et al., 2016). The comparison of DBF with dinocyst concentrations gives an indication of the influence of productivity and/or sedimentation rate on the observed fluctuations. If DBF and dinocyst concentration show the same pattern, the changes in concentrations can be interpreted to reflect changes in productivity (Hennissen et al., 2014).

3.3.2. Acritarchs

Acritarchs are indicators for marine productivity, stratification, and/or water temperature (De Schepper & Head, 2014; de Vernal & Mudie, 1989a, 1989b; Schreck et al., 2013). The acritarch burial flux was calculated based on the formula:

$$\mathrm{ABF} = C_A \times \rho \times S \quad (2)$$

with acritarch burial flux (ABF) in acritarchs/(cm^2 ka), C_A representing the acritarch concentration (cysts/g), ρ the dry bulk density (g/cm^3), and S the sedimentation rate (cm/ka).

4. Results

4.1. Dinoflagellate Cyst Assemblages

In ODP Hole 642B, 71 dinocyst taxa were encountered in the Piacenzian sediments, with the 11 most abundant taxa always comprising at least 80% of the assemblage in any sample (Figure 2). The number of taxa in any one sample ranges between 19 and 34. Four taxa, namely, cysts of *Protoceratium reticulatum*, *Filisphaera filifera*, *Habibacysta tectata*, and *Spiniferites*/*Achomosphaera* spp. constitute between 52 and 87% of the assemblages. Other rare to common species include *Bitectatodinium raedwaldii*, *B. tepikiense*, *Lingulodinium machaerophorum*, *Impagidinium pallidum*, *Nematosphaeropsis labyrinthus*, *Pyxidinopsis braboi*, and Round Brown Cysts.

Cysts of *P. reticulatum*, *F. filifera*, and *H. tectata* show marked relative abundance changes over the studied time interval (3.320 and 3.137 Ma), covering MIS M2 to the early part of MIS KM2 (Figure 2). During MIS M2, relative abundances of cysts of *P. reticulatum* are relatively constant between ~25 and 40%. Proportions of *F. filifera* are higher in the first half of MIS M2, with values around 10–15%, and decline to values of <10% after 3.284 Ma. Relative abundances of cysts of *P. reticulatum* decline throughout MIS M1,

Table 1
Taxonomic Names of Dinoflagellate Cyst and Acritarch Taxa (Following De Schepper & Head, 2008, 2014; Head, 1996; Head et al., 1989; Williams et al., 2017) From the Mid-Piacenzian of ODP Hole 642B

Dinoflagellate cysts
Achomosphaera andalousiensis
Achomosphaera andalousiensis subsp. *andalousiensis*
Achomosphaera andalousiensis subsp. *suttonensis*
Achomosphaera ramulifera
Amiculosphaera umbraculum
Ataxiodinium choane
Ataxiodinium spp.
Ataxiodinium zevenboomii
Barssidinium spp.
Barssidinium graminosum
Barssidinium pliocenicum
Batiacasphaera micropapillata
Bitectatodinium raedwaldii
Bitectatodinium? *serratum*
Bitectatodinium sp. A of De Schepper et al. (2017)
Bitectatodinium spp.
Bitectatodinium tepikiense
Brigantedinium spp.
cf. *Cerebrocysta*? *namocensis*
Corrudinium harlandii
Corrudinium? *labradori*
Corrudinium spp.
Cyst of *Pentapharsodinium dalei*
Cysts of *Protoceratium reticulatum*
Dapsilidinium pseudocolligerum
Echinidinium spp.
Filisphaera filifera
Filisphaera microornata
Filisphaera spp.
Habibacysta tectata
Heteraulacacysta sp. A of Costa and Downie (1979)
Impagidinium aculeatum
Impagidinium pallidum
Impagidinium paradoxum
Impagidinium patulum
Impagidinium solidum
Impagidinium sp. 2 of De Schepper and Head (2009)
Impagidinium spp.
Invertocysta lacrymosa
Invertocysta sp. 1 (this study)
Invertocysta spp.
Lejeunecysta catomus?
Lingulodinium machaerophorum
Melitasphaeridium choanophorum
Melitasphaeridium sp. A of De Schepper and Head (2008)
Melitasphaeridium spp.
Nematosphaeropsis labyrinthus
Nematosphaeropsis lativittata
Nematosphaeropsis spp.
Operculodinium? *eirikianum* var. *eirikianum*
Operculodinium centrocarpum s.s.
Operculodinium janduchenei
Operculodinium sp.
Pyxidinopsis braboi
Round brown cysts
Selenopemphix conspicua
Selenopemphix dionaeacysta
Selenopemphix cf. *islandensis*
Selenopemphix nephroides

Table 1 *(continued)*

Dinoflagellate cysts
Selenopemphix nephroides - small variety (c. 20μm, this study)
Spiniferites elongatus
Spiniferites falcipedius
Spiniferites mirabilis
Spiniferites membranaceus
Spiniferites ramosus
Spiniferites/Achomosphaera spp.
Tectatodinium pellitum
Trinovantedinium glorianum
Trinovantedinium spp.
Tuberculodinium vancampoae
Dinocyst spp.
Acritarchs
Cymatiosphaera? *aegirii*
Cymatiosphaera? *fensomei*
Cymatiosphaera? *icenorum*
Cymatiosphaera? *invaginata*
Lavradosphaera canalis
Lavradosphaera crista
Nannobarbophora walldalei

before reaching minimum values of 8% in the first half of MIS KM6. At the start of MIS M1, percentages of *F. filifera* show a marked increase from 4 to 12% with values increasing to a maximum of 25% at 3.228 Ma within the early part of MIS KM6. Proportions of *H. tectata* are very low (<4%) during MIS M2 but gradually increase throughout MIS M1 and reach values of up to 29% in the first half of MIS KM6. In the middle of MIS KM6 between 3.225 and 3.222 Ma, a sharp increase in the relative abundances of cysts of *P. reticulatum* from 13 to 48% occurs, which is accompanied by a marked decline in the relative abundances of *F. filifera* and *H. tectata*. Subsequently, relative abundances of cysts of *P. reticulatum* gradually increase to maximum values of 64% at 3.205 Ma within MIS KM5, while *F. filifera* and *H. tectata* both show proportions of less than 7%. After 3.205 Ma, relative abundances of cysts of *P. reticulatum* continuously decline. Proportions of *F. filifera* peak at 3.189 and 3.179 Ma and stay around 5–10% until values drop to <3% at 3.142 Ma within MIS KM2. A clear increase in the relative abundance of *H. tectata* occurs at 3.185 Ma at the end of MIS KM5, continuing throughout MIS KM4 and reaching highest values of 32% at 3.159 Ma in the middle of MIS KM3. Afterward, proportions of *H. tectata* decline and those of *L. machaerophorum* increase to up to 16%.

Cyst concentrations range between 500 and 5,500 cysts/g in the majority of samples (Figure 2). Highest concentrations occur between 3.222 and 3.197 Ma with maximum values of 13,000 cysts/g at 3.203 Ma. The DBF shows the same pattern as the cyst concentrations throughout most of the interval. However, the DBF declines sharply between 3.214 and 3.207 Ma, while cyst concentrations remain high until 3.197 Ma (Figure 2).

4.2. Acritarch Assemblages

In the analyzed samples, the total counts of acritarchs range between 28 and 1,099 and the proportion of acritarchs in the total marine palynological assemblage (dinocysts and acritarchs) varies between 7 and 74%. Twelve taxa and taxa groups are differentiated, with seven taxa having been formally described (Table 1). Five taxa, namely, *Cymatiosphaera*? *icenorum*, *C.*? *invaginata*, *Lavradosphaera crista*, *Nannobarbophora walldalei*, and small spiny acritarchs are abundant to dominant in Hole 642B. Acritarch concentrations are comparable to dinocyst concentrations for most of the studied interval with values fluctuating between ~140 and 1400 acritarchs/g. Maximum concentrations of ~16,400–21,300 acritarchs/g are reached between 3.217 and 3.205 Ma (Figure 3). The ABF shows a good correlation to the acritarch concentration with the exception of the early part of MIS KM5, when the ABF declines before the concentration decreases (Figure 2).

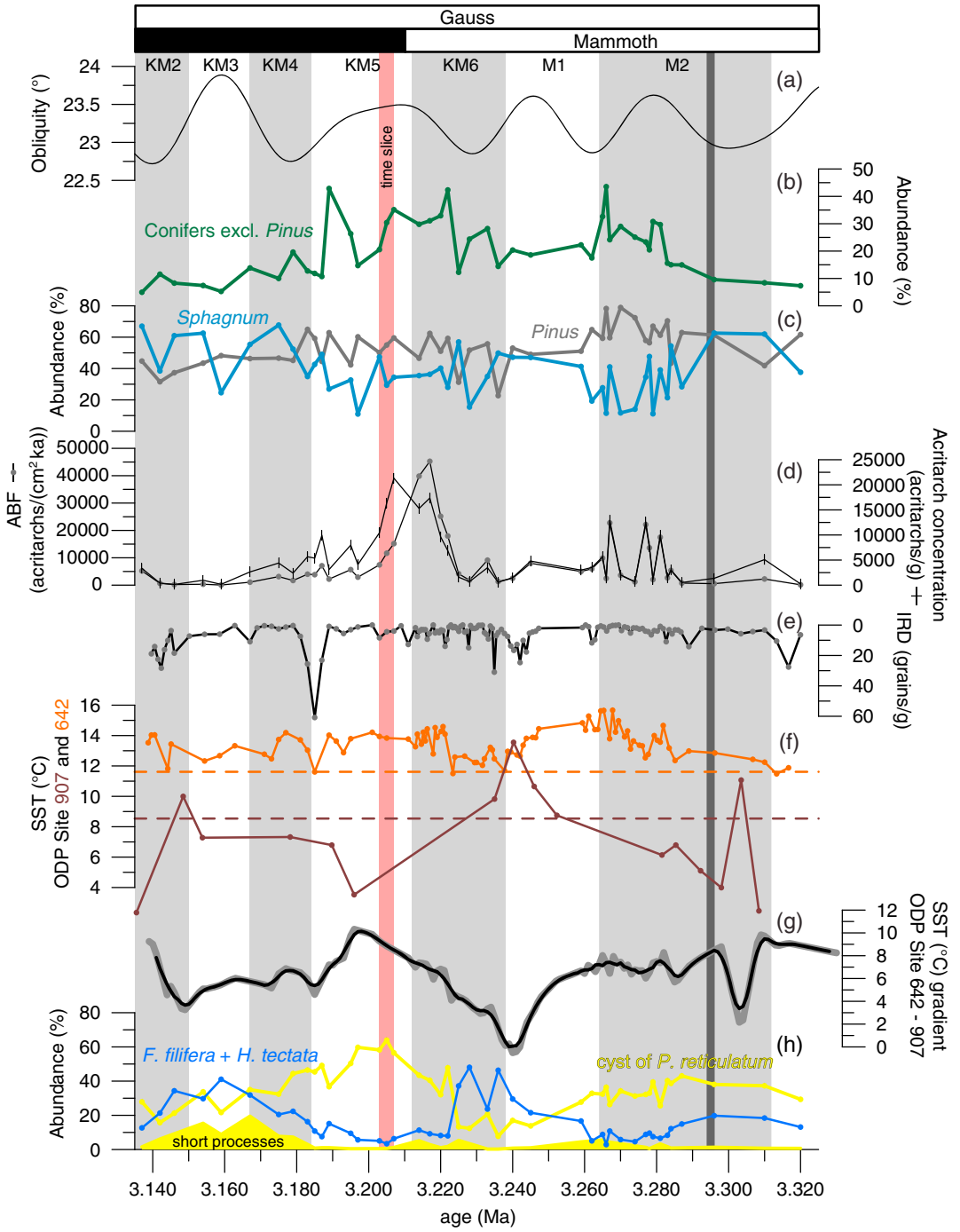

Figure 3. Paleoceanographic and paleoterrestrial proxy records from ODP Hole 642B in the Norwegian Sea. (a) Obliquity after Laskar et al. (2004); (b, c) conifer taxa excluding *Pinus* (green), relative abundances of *Pinus* pollen (gray) and *Sphagnum* spores (blue); (d) acritarch burial flux (ABF, line with gray dots) and total acritarch concentration (line with vertical bars); (e) ice rafted debris (IRD) concentrations; (f) alkenone-based sea surface temperature (SST) estimates for ODP Hole 642B (orange, solid line) (Bachem et al., 2017) and Holocene mean SST at nearby Site MD95–2011 (orange, dashed line) (Calvo et al., 2002), and alkenone-based SSTs for ODP Hole 907A (brown, solid line) [this study] and Holocene mean SST at nearby Site GS15-198-62 MC-A (brown, dashed line) (Bachem et al., 2017); (g) SST gradient (gray shading) between Site 642 and 907 calculated by subtracting the records after interpolating to 1 kyr resolution. Black line is the 5-point running average; (h) relative abundance of cysts of *P. reticulatum* (yellow line), cysts of *P. reticulatum* with short processes (filled yellow area), *F. filifera* (light blue) and *H. tectata* (dark blue). Dark gray vertical bar indicates the possible presence of an hiatus over the most extreme part of marine isotope stage M2 (Risebrobakken et al., 2016). Light red bar marks the KM5c time slice chosen for data-model comparison (Haywood, Dolan, et al., 2013).

5. Discussion

5.1. Paleoecology of the Dominant Dinoflagellate Cyst Species in ODP Hole 642B

Of the three most abundant dinocyst species (cysts of *P. reticulatum*, *F. filifera*, and *H. tectata)* in the mid-Piacenzian sediments of Hole 642B, only cysts of *P. reticulatum* are still extant. This species is cosmopolitan, tolerates a wide range of temperature and salinity (Zonneveld et al., 2013), can be abundant near shelf edges (Dale & Dale, 2002; Wall et al., 1977), and is usually overrepresented in fossil assemblages due to high cyst production (Bolch & Hallegraeff, 1990; Dale, 1976). Nevertheless, in the modern North Atlantic, cysts of *P. reticulatum* are recorded in high abundance (up to 91%) along the path of the NAC (Rochon et al., 1999; Zonneveld et al., 2013). Atlantic water flows into the Nordic Seas via the NwAC, which is reflected in abundances of this species above 60% in modern dinocyst assemblages in the Norwegian Sea (Matthiessen, 1995). In pre-Quaternary paleoceanographic reconstructions in the North Atlantic and Nordic Seas, cysts of *P. reticulatum* have been used as a tracer of Atlantic water because of their modern association with the NAC and NwAC (De Schepper et al., 2013, 2015; Grøsfjeld et al., 2009; Hennissen et al., 2014; Knies, Mattingsdal, et al., 2014). Given that the major transport of Atlantic water in the Norwegian Sea occurs via the northward flowing NwAC, distinct variations in the abundances of cysts of *P. reticulatum* in Hole 642B are interpreted to indicate changes in the inflow of Atlantic water into the Norwegian Sea.

Both *F. filifera* and *H. tectata* became extinct during the Pleistocene (Head, 1996). According to their stratigraphic records, these species have previously been classified as cold-water tolerant species as they are common elements of Pliocene high-latitude sites in the Northern Hemisphere (Head, 1994, 1996). However, the high latitudes were markedly warmer than today during the Pliocene (Bachem et al., 2017; De Schepper et al., 2015; Herbert et al., 2016), suggesting that these species could live in relatively mild SSTs. During the Pliocene/Pleistocene, percentages of *F. filifera* above 5% are associated with Mg/Ca-based (*Globigerina bulloides*) spring-summer SSTs of $>$11°C and abundances of *H. tectata* $>$ 30% with spring-summer SSTs between 10 and 16°C (Mg/Ca, *G. bulloides*) in the eastern North Atlantic (De Schepper et al., 2011; Hennissen et al., 2017). At Deep Sea Drilling Project Site (DSDP) Site 610 in the eastern North Atlantic, *F. filifera* occurs in higher abundances (up to 8%) during glacial MIS M2 (De Schepper, Head, & Groeneveld, 2009), reflecting its affinity for cool waters. During the intensification of Northern Hemisphere Glaciation across the Pliocene/Pleistocene transition, higher abundances (up to 53%) of *H. tectata* are recorded during cooler intervals when proportions of cysts of *P. reticulatum* are relatively low due to shifts in the NAC (Hennissen et al., 2014, 2017). In Hole 642B, *F. filifera* and *H. tectata* might be characteristic elements of the dinocyst assemblage during the Piacenzian given their continuous presence throughout the studied interval and the location of the site just north of the Arctic Circle.

Other potential cool-water indicators that are continuously present in low abundances in the Hole 642B record include the extant species *Bitectatodinium tepikiense* and *Impagidinium pallidum* (Figure 2). In the modern ocean, *B. tepikiense* is restricted to subarctic to temperate waters (Zonneveld et al., 2013). During the Pliocene/Pleistocene, the relationship between abundances of *B. tepikiense* and Mg/Ca-based (*G. bulloides*) spring-summer paleo-SSTs in the North Atlantic compares closely to present (De Schepper et al., 2011; Hennissen et al., 2017). At present, *I. pallidum* is a bipolar species mostly encountered in cold surface waters but its presence at North Atlantic sites during the Pliocene suggests a tolerance of a wide temperature range, limiting the use of this species as a paleotemperature indicator (De Schepper et al., 2011; Hennissen et al., 2017).

Species of *L. machaerophorum* are presently mainly found in coastal temperate to equatorial regions with summer temperatures above 10°C (Zonneveld et al., 2013). During the late Piacenzian, *L. machaerophorum* is a common element in the palynomorph assemblages deposited in the southern North Sea Basin, where it has been used as an indicator for warm temperate conditions (De Schepper, Head, & Louwye, 2009; Head, 1998). The species tolerates a broad range of salinity and also occurs in high abundances near upwelling cells, below river plumes or in highly stratified waters (Zonneveld et al., 2013). In Norwegian fjords, higher numbers of this species have been associated with increased eutrophication (Dale et al., 1999; Thorsen & Dale, 1997).

To better interpret the dinocyst assemblage response to surface circulation changes and particularly to SST changes associated with variations in the influence of Atlantic and Arctic water at Site 642, we calculated the gradient between SSTs from Site 642 (Bachem et al., 2017) and Site 907 in the Iceland Sea [this study]

(Figures 1 and 3). The reconstruction of this gradient is limited by the lower sampling resolution in Hole 907A, but the absolute values as well as the trend in SST changes is supported by a low-resolution alkenone SST record from the same site (Herbert et al., 2016). A strong gradient can be seen as an indication for the presence of a proto-Artic Front (AF) between the Iceland and Norwegian Sea comparable to the modern situation, while a weak or absent gradient suggests the absence of a proto-AF between both sites. For most of the studied interval, the SST gradient fluctuates around or exceeds ~5–8°C, suggesting that a proto-AF was present (Figure 3). Under these conditions, abundances of cysts of *P. reticulatum* fluctuate between ~25 and 45%, while the combined proportions of *F. filifera* and *H. tectata* do not exceed ~25% (Figure 3). Around 3.24 Ma, the gradient drops to ~0°C, mainly due to warming in the Iceland Sea (Figure 3), indicating an AF likely did not exist between the sites. This is associated with the lowest percentages (~10%) of cysts of *P. reticulatum* within the studied interval and highest abundances (~50%) of *F. filifera* and *H. tectata*.

5.2. Mid-Piacenzian Paleoceanography of the Norwegian Sea and Links to Terrestrial Environmental Changes

5.2.1. MIS M2 to MIS M1 (3.312–3.264 Ma): From Glacial to Interglacial Conditions

During MIS M2, relative abundances of cysts of *P. reticulatum* around ~30–40% indicate a constant influence of Atlantic and/or shelf water (Figure 2). Abundances of *F. filifera* reach up to 17% during the first half of MIS M2. At the same time, SSTs in Hole 642B are low for the Pliocene and comparable to the Holocene average, with values around 12–13°C (Figure 3) (Bachem et al., 2017), suggesting that *F. filifera* is a common element of the Piacenzian dinocyst assemblage under conditions similar to today. A proto-AF was present between Sites 642 and 907 as indicated by a gradient of ~6–10°C (Figure 3). The predominance of *Pinus* pollen and *Sphagnum* spores in the pollen assemblages of Hole 642B suggests the prevalence of boreal forests and an extensive distribution of peatlands under subarctic, near-modern climatic conditions in northern Norway (Figure 3) (Panitz et al., 2016). Terrestrial climatic conditions might have been cold enough for the establishment of mountain glaciers despite the lower-than-present height of the Scandinavian mountains (Anell et al., 2009; Knies, Mattingsdal, et al., 2014; Panitz et al., 2016).

Glacial MIS M2 has been globally recognized in benthic oxygen isotope and other marine and terrestrial proxy records as a pronounced cooling event during the warmer-than-present Piacenzian (Brigham-Grette et al., 2013; De Schepper et al., 2013, 2014; Lisiecki & Raymo, 2005; Mudelsee & Raymo, 2005). In Hole 642B, MIS M2 is not as distinctly recorded as at other sites in neither environmental changes derived from dinocysts, SSTs, and pollen nor in the benthic oxygen isotope signal (Figures 2 and 3), which suggests that the event might have been less pronounced in the Norwegian Sea area. However, it is likely that the most extreme part of MIS M2 is missing due to a minor hiatus (≤10 kyr) (Risebrobakken et al., 2016) and more records are needed to assess the impact of this global cooling event on the Nordic Seas and Norwegian environment. The marine and terrestrial proxy records from Hole 642B are indicative of Holocene-like climatic conditions in the Norwegian Sea region during the early part of MIS M2, which supports the inference of a similar-to-present Northern Hemisphere ice sheet/glacier volume (De Schepper et al., 2014). At Site 907, the presence of IP_{25} indicates seasonal sea ice cover around 3.3 Ma; an interpretation which is supported by low concentrations of marine biomarkers and SSTs (Clotten et al., 2018). In addition, a pronounced IRD peak suggests that glaciers reached the coastline, calving icebergs in the ocean (Jansen et al., 2000). During the second half of MIS M2, SSTs and productivity increases while the influence of Atlantic water remains unchanged. A decline in the relative abundance of *F. filifera* is observed between 3.284 and 3.281 Ma (Figure 3). This is interpreted to reflect the warming of surface waters as recorded in a rise in SSTs of ~5°C to highest values (~15–16°C) within the studied interval between 3.285 and 3.283 Ma, tracing the obliquity cycle (Figure 3) (Bachem et al., 2017). The ABF also increases between 3.287 and 3.284 Ma, suggesting enhanced marine productivity (Figure 3) (de Vernal & Mudie, 1989b; Schreck et al., 2013). The warming in the Norwegian Sea coincides with a distinct increase in the proportions of thermophilous conifer taxa, such as *Sciadopitys* and *Tsuga*, from 12 to 42% between 3.283 and 3.281 Ma (Figure 3). This is indicative of the establishment of diverse, cool temperate mixed forests, and warmer-than-present climatic conditions in northern Norway (Panitz et al., 2016). With the warming being most pronounced in the SST record from Hole 642B and vegetation changes in northern Norway (Bachem et al., 2017; Panitz et al., 2016), it is likely a response to increased obliquity forcing, which strengthened the seasonal contrast and led to warm summers (e.g., Haug et al., 2001).

5.2.2. MIS M1 Toward KM6: Establishment of Cooler Climatic Conditions

At approximately 3.260 Ma, the abundance of *F. filifera* increases and is comparable to the first half of MIS M2, suggesting similar-to-present oceanographic conditions established (Figure 2). This is supported by the presence of a proto-AF as indicated by a SST gradient of ~6°C between sites 642 and 907 (Figure 3). The increase in proportions of *F. filifera* is accompanied by an increase in the relative abundance of *Sphagnum* spores and low proportions of thermophilous conifers, indicating an expansion of peatlands at the expense of forests and the establishment of subarctic climatic conditions in northern Norway (Panitz et al., 2016). For the middle section of MIS M1 no sediment was available for analysis. Above the sampling gap, the relative abundance of cysts of *P. reticulatum* declines toward MIS KM6 which is interpreted as a reduction of Atlantic water influence via the NwAC. This is supported by low concentrations and influxes of dinocysts, and acritarchs (Figures 2 and 3), indicating reduced marine productivity and a cooling of surface waters at Site 642 (Figure 3). The decrease of SSTs after 3.247 Ma traces the obliquity cycle (Bachem et al., 2016), suggesting that the weakened seasonality and warmer winters might have contributed to a reduction in the NwAC influence. At the same time, relatively high abundances of *Sphagnum* spores and *Pinus* pollen are indicative of subarctic climatic conditions on land (Figure 3). While SSTs decrease in the Norwegian Sea, a pronounced warming of surface waters is recorded in the Iceland Sea, suggesting a collapse of the SST gradient and the absence of a proto-AF between Sites 642 and 907 (Figure 3). This is indicative of a weakened NwAC and EGC in the Nordic Seas, with Site 907 being influenced by warmer, presumably Atlantic waters, entering through the Denmark Strait. It also suggests that an active NwAC is needed for an AF to develop between the Norwegian and Iceland Sea. The good correlation of dinocyst and pollen assemblage changes suggests that a reduced Atlantic water influence due to the absence of the NwAC had a direct impact on terrestrial climate.

5.2.3. MIS KM6 (3.238–3.212 Ma): Increased Inflow of Warm Atlantic Waters

The cooling that commenced within MIS M1 culminates during the first half of MIS KM6, which is evident in peaks in the abundances of *F. filifera* and *H. tectata* (Figure 2), following the reduction of NwAC influence. This is also reflected in Holocene-like SSTs in Hole 642B (Figure 3) (Bachem et al., 2016). Between 3.225 and 3.222 Ma, a distinct increase in the relative abundance (up to ~48%) and concentrations of cysts of *P. reticulatum* takes place (Figure 2), indicating increased inflow of Atlantic waters into the Norwegian Sea. The increase in abundance of cysts of *P. reticulatum* also corresponds to an increase in the total DBF and ABF (Figures 2 and 3), suggesting that nutrient-rich water influenced the site and led to enhanced productivity. An increase in SSTs in Hole 642B by ~2.5°C is recorded at 3.223 Ma (Figure 3) (Bachem et al., 2016). Bachem et al. (2016) note that the rise in SSTs coincides with an increase in obliquity, indicating that the warming might be a response to orbital forcing. However, the abrupt increase in the abundance of cysts of *P. reticulatum* prior to a rise in SSTs suggests that the latter is at least partly, if not entirely, controlled by water mass changes not linked to obliquity changes. The oceanographic change coincides with an increase in the proportions of *Pinus* and other conifer pollen, reflecting a change from boreal to cool temperate climatic conditions. The contemporaneous change of water masses and vegetation is indicative of an immediate response of the latter to oceanographic changes.

5.2.4. MIS KM5 (3.212–3.184 Ma): Warmer-Than-Present Interglacial Conditions

Relative abundances of cysts of *P. reticulatum* increase continuously to maximum values of ~64% at 3.205 Ma, with high proportions predominating until 3.197 Ma, suggesting an increased influence of Atlantic water via a well-established NwAC (Figure 2). This is supported by the low proportions of the cold-water tolerant taxa *F. filifera* (<11%) and *H. tectata* (<9%). Increased Atlantic water influence in the Norwegian Sea and SSTs ~2°C higher when compared to the Holocene average (Bachem et al., 2016) coincide with relatively low SSTs in the Iceland Sea [this study], resulting in a strong SST gradient and thus the presence of a proto-AF between sites 642 and 907 (Figure 3). The overall high percentages of cool temperate pollen taxa are in line with warmer-than-present climatic conditions (Figure 3).

At the end of MIS KM5, the relative abundance of conifer taxa excluding *Pinus* declines after peaking at 3.189 Ma (Figure 3), indicating a shift toward predominantly boreal forests and subarctic climatic conditions in northern Norway. This cooling corresponds to a drop in SSTs of ~2°C in Hole 642B between 3.189 and 3.185 Ma and a contemporaneous increase in IRD, most likely originating from sea-terminating ice masses on Greenland (Figure 3) (Bachem et al., 2016). This cooling on land is not reflected in the dinocyst assemblage changes, indicating stable water masses and a change in marine and terrestrial surface temperature, possibly driven by weakened obliquity and insolation forcing (Figures 2 and 3). However, while SSTs return to values

comparable to those before the cooling event, abundances of cool temperate pollen taxa remain low, suggesting that subarctic climatic conditions persisted in northern Norway.

5.2.5. MIS KM4–KM2 (3.184–3.137 Ma): Cooling of the Sea and Land

Declining abundances of cysts of *P. reticulatum* and increasing proportions of *H. tectata* are indicative of a reduced influence of Atlantic water after 3.189 Ma (Figure 3). During MIS KM4 and KM3, a freshening of the water masses, when compared to the previous intervals, may be inferred from higher proportions of cysts of *P. reticulatum* with short processes (Figure 3). In the modern North Atlantic Ocean, the process length of this species shows a positive correlation to sea surface salinity and density (Jansson et al., 2014; Mertens et al., 2010, 2012). Hole 642B SSTs only show low-amplitude changes, with values fluctuating between 12 and 14°C (Figure 3) (Bachem et al., 2016). Both pollen of *Pinus* and other conifer taxa show low (<13%) and decreasing abundances throughout MIS KM4 to KM2, reflecting the prevalence of boreal forest and a continuous decline in forest cover in northern Norway. Proportions of *Sphagnum* spores reach values as high as those during the early part of MIS M2 but are still variable, indicating a repeated expansion of peatlands at the expense of forest under subarctic climatic conditions (Figure 3) (Panitz et al., 2016).

During MIS KM2, the increase in the abundances of *L. machaerophorum* suggests an influence of an additional water mass, or change in taphonomy (Figure 2). The higher abundances of *L. machaerophorum* are unlikely to be linked to increased nutrient availability due to the contemporaneous low proportions of cysts of *P. reticulatum*, RBCs, and low DBF and ABF rates (Figure 2). As *L. machaerophorum* is a typical neritic species, restricted to the coastal regions and vicinity of continental margins (Zonneveld et al., 2013), the higher abundances in Hole 642B during MIS KM2 might be an indication of an increased influence of water from the inner shelf area. The process length of *L. machaerophorum* has also been correlated with salinity (Mertens et al., 2009; Verleye et al., 2009). In this study, specimens with reduced processes were identified in the samples with high abundances of this species but not quantified. Thus, the cysts might have been produced in fresher, inner shelf water, and transported to the site.

5.3. Norwegian Sea-North Atlantic Water Mass Exchange During the MIS M2/M1 Transition

In the eastern North Atlantic, Piacenzian oceanographic changes have been inferred from dinocyst assemblage changes at DSDP Site 610, International Ocean Drilling Program (IODP) Site U1308, and IODP Site U1313 (Figure 1) (De Schepper et al., 2013; Hennissen et al., 2014). The transition between full-glacial conditions during MIS M2 and interglacial MIS M1 has been suggested to represent a climatic evolution from glacial, similar-to-modern to warmer-than-present conditions driven by a reinvigoration of the NAC in the North Atlantic around 3.285 Ma and accompanied increase in northward heat transport (De Schepper et al., 2013; Naafs et al., 2010). During MIS M2, cysts of *P. reticulatum* are present in very low abundances at Site 610 and Site U1308, indicating the absence of northward warm water transport via the NAC (De Schepper et al., 2013). If a hiatus over parts of MIS M2 can be excluded in Hole 642B, relatively high proportions of this species during MIS M2 (Figure 2) suggest either that Atlantic water influence prevailed or that its local representation is affected by other factors than the influence of Atlantic water. These factors include influx of cysts from the shelf edge (Dale & Dale, 2002) and/or higher cyst productions in comparison to other species (Dale, 1976). During the first half of MIS M2, cool climatic conditions persisted in the Norwegian Sea, with high abundances of *F. filifera*, Holocene-like SSTs (Bachem et al., 2016) and a strong SST gradient between sites 642 and 907 (Figure 3), indicating the presence of a proto-AF and similar-to-present oceanographic conditions. At the same time, the presence of boreal vegetation in northern Norway also resembles modern climatic conditions (Figure 3) (Panitz et al., 2016).

In the eastern North Atlantic, warming at 3.285 Ma is seen in SST reconstructions as well as an increase in the relative abundance of cysts of *P. reticulatum* at Site 610 and Site U1308 (De Schepper et al., 2013). In Hole 642B, the warming is not associated with an increase in the proportions of this species but is instead evident in a decline in the abundances of *F. filifera*. The warming is particularly pronounced in an increase of SSTs in the Norwegian Sea (Bachem et al., 2017), which barely affects the SST gradient between Sites 642 and 907 due to a contemporaneous warming in the Iceland Sea (Figure 3). In northern Norway, cool temperate climatic conditions establish at 3.283 Ma. Together, the changes suggest that the prevalence of cysts of *P. reticulatum* is an expression of constant Atlantic water influence and possibly the site location close to the Norwegian shelf edge. In addition, the SST increase and vegetation changes mainly seem to be a response to obliquity forcing which does not affect the NwAC. Thus, the warming in the Norwegian Sea, marking the

MIS M2/M1 transition, is presumably mainly the result of a strengthened seasonal contrast with warmer summers due to increased obliquity (e.g., Haug et al., 2005). With the inflow of Atlantic water into the Nordic Seas being constrained to the Iceland-Faroe Ridge and Faroe-Shetland Channel, changes in the position of the NAC during the MIS M2/M1 transition might be restricted to the North Atlantic (De Schepper et al., 2013).

5.4. Paleoenvironmental Conditions During the Pliocene Time Slice (3.205 Ma)

To address the discrepancy in the magnitude of warming between proxy-based climate reconstructions and model simulations during the mid-Piacenzian, a time slice centered on 3.205 Ma (3.204–3.207 Ma) has been chosen within the warm period to overcome the problem of warm peak averaging (Haywood, Dolan, et al., 2013). The time slice falls on a prolonged negative isotope excursion (MIS KM5c) to ensure warmer-than-present climatic conditions and coincides with an interval characterized by relatively stable orbital forcing, comparable to the preindustrial, to reduce the influence of other forcings than higher atmospheric CO_2 concentrations (Haywood, Dolan, et al., 2013).

In Hole 642B, highest abundances of cysts of *P. reticulatum* within the studied interval occur at 3.205 Ma (Figure 2), indicating the presence of a well-established NwAC and maximum influence of Atlantic water. At the same time, SSTs are relatively high and stable, fluctuating around 14°C (Figure 3), which is in line with low-amplitude changes in obliquity (Bachem et al., 2016). Cool temperate pollen taxa show relatively high abundances between 3.207 and 3.205 Ma (Figure 3), suggesting the presence of mixed forests and warmer-than-present climatic conditions in northern Norway. A pronounced SST gradient between Sites 642 and 907 (Figure 3) is indicative of the presence of a proto-AF and strong surface circulation in the Nordic Seas, that is, a well-established NwAC and EGC. It is notable, however, that the time slice only stands out in the dinocyst record relative to the signal seen during the other mid-Piacenzian interglacials (Figure 3).

The high-resolution, multiproxy record from Hole 642B highlights high-frequency, low-amplitude climate variability during the mid-Piacenzian, with climatic conditions fluctuating between warmer-than-present and similar-to-modern in the Norwegian Sea region. This study underlines the value of focusing on a time slice for data-model comparison to reduce uncertainties related to regional climate variability.

6. Conclusions

This study integrates a new mid-Piacenzian record of dinocyst assemblage changes from ODP Hole 642B in the Norwegian Sea with an alkenone and pollen and spore record from the same site to investigate the link between surface water masses, SSTs, and terrestrial climate. Our study shows regional climate changes in response to variations in northward heat transport via the NwAC and/or obliquity forcing. We identified five major climate changes in the Norwegian Sea and on the Scandinavian mainland:

1. MIS M2/M1: Similar-to-present oceanographic and terrestrial conditions prevail during the first half of MIS M2. The end of MIS M2 is characterized by warming of surface waters at approximtely 3.283 Ma which is accompanied by a change from boreal to cool temperate vegetation in northern Norway. The dinocyst record indicates no change of the NwAC, suggesting a constant inflow of Atlantic water into the Norwegian Sea and obliquity changes as the main driver of the warming.
2. MIS M1: During the early part of MIS M1, cooling leads to the reestablishment of climatic conditions comparable to present and boreal vegetation in northern Norway.
3. MIS KM6/KM5: The cooling recorded in the dinocyst and pollen record that commenced at the beginning of MIS M1 culminates in the first half of MIS KM6. A weak surface ocean circulation appears to prevail in the Nordic Seas as seen in the absence of a zonal gradient between the Norwegian and Iceland Sea. The NwAC might have weakened in response to warmer winters as a result of reduced obliquity. A strong increase in marine and terrestrial surface temperatures at approximately 3.222 Ma correlates with strengthened obliquity forcing. However, the dinocyst record indicates that a contemporaneous increase in northward heat transport via the NwAC may have also played an important role.
4. MIS KM5c: The influence of the NwAC is strongest within the studied time interval, resulting in a strong SST gradient between the Norwegian and Iceland Sea and thus a enhanced surface ocean circulation. Alkenone-derived SSTs in the Norwegian Sea are ~2°C higher than the Holocene average and warmer-than-present climatic conditions prevail in northern Norway.
5. MIS KM4–KM2: A reduced influence of the NwAC is accompanied by relatively cool SSTs and the establishment of boreal vegetation and subarctic climatic conditions in northern Norway.

Our study demonstrates the importance of using assemblage studies and linking evidence from both marine and terrestrial proxies to better understand how ocean currents and orbital forcing control climate variability of the high latitudes in a warmer-than-present world.

Acknowledgments
We acknowledge the International Ocean Drilling Program for providing the samples. We thank M. Jones (Palynological Laboratory Services LtD) and L. Dunlop (Northumbria University) for their help with the preparation of samples. The work is a contribution to the "Ocean Controls on high-latitude Climate sensitivity—a Pliocene case study" (OCCP) project funded by the Norwegian Research Council (project 221712). S. D. S. is grateful for support from the Norwegian Research Council (project 229819). S. P. acknowledges funding received from the European Consortium for Ocean Research Drilling (ECORD). The dinocyst data presented here are available in the supporting information and the alkenone SST for ODP Site 907 at https://doi.pangaea.de/10.1594/PANGAEA.877309. We thank J. Matthiessen and H. Dowsett for the constructive comments on the manuscript.

References

Anell, I., Thybo, H., & Artemieva, I. M. (2009). Cenozoic uplift and subsidence in the North Atlantic region: Geological evidence revisited. *Tectonophysics*, *474*, 78–105. https://doi.org/10.1016/j.tecto.2009.04.006

Bachem, P. E., Risebrobakken, B., De Schepper, S., & McClymont, E. L. (2017). Highly variable Pliocene sea surface conditions in the Norwegian Sea. *Climate of the Past*, *13*(9), 1153–1168. https://doi.org/10.5194/cp-13-1153-2017

Bachem, P. E., Risebrobakken, B., & McClymont, E. L. (2016). Sea surface temperature variability in the Norwegian Sea during the late Pliocene linked to subpolar gyre strength and radiative forcing. *Earth and Planetary Science Letters*, *446*, 113–122. https://doi.org/10.1016/j.epsl.2016.04.024

Badger, M. P. S., Schmidt, D. N., Mackensen, A., & Pancost, R. D. (2013). High-resolution alkenone palaeobarometry indicates relatively stable pCO_2 during the Pliocene (3.3–2.8 Ma). *Philosophical Transactions. Series A, Mathematical, Physical, and Engineering Sciences*, *371*(2001), 20130094. https://doi.org/10.1098/rsta.2013.0094

Bartoli, G., Hönisch, B., & Zeebe, R. E. (2011). Atmospheric CO_2 decline during the Pliocene intensification of Northern Hemisphere glaciations. *Paleoceanography*, *26*, PA4213. https://doi.org/10.1029/2010PA002055

Bleil, U. (1989). Magnetostratigraphy of Neogene and Quaternary sediment series from the Norwegian Sea: Ocean Drilling Program, Leg 104. *Proceedings. Ocean Drilling Program. Scientific Results*, *104*, 829–901.

Blindheim, J., & Østerhus, S. (2005). The Nordic Seas, main oceanographic features. *Geophysical Monograph Series*, *158*, 11–37. https://doi.org/10.1029/158GM03

Bolch, C. J., & Hallegraeff, G. M. (1990). Dinoflagellate cysts in recent marine sediments from Tasmania, Australia. *Botanica Marina*, *33*(2), 173–192. https://doi.org/10.1515/botm.1990.33.2.173

Brigham-Grette, J., Melles, M., Minyuk, P., Andreev, A., Tarasov, P., DeConto, R., … Herzschuh, U. (2013). Pliocene warmth, polar amplification, and stepped Pleistocene cooling recorded in NE Arctic Russia. *Science*, *340*(6139), 1421–1427. https://doi.org/10.1126/science.1233137

Calvo, E., Grimalt, J., & Jansen, E. (2002). High resolution UK37 sea surface temperature reconstruction in the Norwegian Sea during the Holocene. *Quaternary Science Reviews*, *21*(12-13), 1385–1394. https://doi.org/10.1016/S0277-3791(01)00096-8

Clotten, C., Stein, R., Fahl, K., & De Schepper, S. (2018). Seasonal sea ice cover during the warm Pliocene: Evidence from the Iceland Sea (ODP Site 907). *Earth and Planetary Science Letters*, *481*, 61–72. https://doi.org/10.1016/j.epsl.2017.10.011

Costa, L., & Downie, C. (1979). Cenozoic dinocyst stratigraphy of Sites 403 to 406 (Rockall Plateau), IPOD, Leg 48. In L. Montadert & D. G. Roberts, *Deep Sea Drilling Project, Initial Reports* (Vol. 48, pp. 513–529).

Dale, B. (1976). Cyst formation, sedimentation, and preservation: Factors affecting dinoflagellate assemblages in recent sediments from Trondheimsfjord, Norway. *Review of Palaeobotany and Palynology*, *22*(1), 39–60. https://doi.org/10.1016/0034-6667(76)90010-5

Dale, B., & Dale, A. L. (2002). Environmental applications of dinoflagellate cysts and acritarchs. In S. K. Haslett (Ed.), *Quaternary Environmental Micropalaeontology* (pp. 207–240). London: Arnold.

Dale, B., Thorsen, T. A., & Fjellsa, A. (1999). Dinoflagellate cysts as indicators of cultural eutrophication in the Oslofjord, Norway. *Estuarine, Coastal and Shelf Science*, *48*(3), 371–382. https://doi.org/10.1006/ecss.1999.0427

De Schepper, S., Beck, K. M., & Mangerud, G. (2017). Late Neogene dinoflagellate cyst and acritarch biostratigraphy for Ocean Drilling Program Hole 642B, Norwegian Sea. *Review of Palaeobotany and Palynology*, *236*, 12–32. https://doi.org/10.1016/j.revpalbo.2016.08.005

De Schepper, S., Fischer, E. I., Groeneveld, J., Head, M. J., & Matthiessen, J. (2011). Deciphering the palaeoecology of late Pliocene and early Pleistocene dinoflagellate cysts. *Palaeogeography Palaeoclimatology Palaeoecology*, *309*, 17–32. https://doi.org/10.1016/j.palaeo.2011.04.020

De Schepper, S., Gibbard, P. L., Salzmann, U., & Ehlers, J. (2014). A global synthesis of the marine and terrestrial evidence for glaciation during the Pliocene epoch. *Earth-Science Reviews*, *135*, 83–102. https://doi.org/10.1016/j.earscirev.2014.04.003

De Schepper, S., Groeneveld, J., Naafs, B. D. A., Van Renterghem, C., Hennissen, J., Head, M. J., … Fabian, K. (2013). Northern Hemisphere glaciation during the globally warm early late Pliocene. *PLoS One*, *8*(12), e81508. https://doi.org/10.1371/journal.pone.0081508

De Schepper, S., & Head, M. J. (2008). New dinoflagellate cyst and acritarch taxa from the Pliocene and Pleistocene of the eastern North Atlantic (DSDP Site 610). *Journal of Systematic Palaeontology*, *6*(1), 101–117. https://doi.org/10.1017/S1477201907002167

De Schepper, S., & Head, M. J. (2009). Pliocene and Pleistocene dinoflagellate cyst and acritarch zonation of DSDP Hole 610A, eastern North Atlantic. *Palynology*, *33*(1), 179–218. https://doi.org/10.2113/gspalynol.33.1.179

De Schepper, S., & Head, M. J. (2014). New late Cenozoic acritarchs: Evolution, palaeoecology and correlation potential in high latitude oceans. *Journal of Systematic Palaeontology*, *12*(4), 493–519. https://doi.org/10.1080/14772019.2013.783883

De Schepper, S., Head, M. J., & Groeneveld, J. (2009). North Atlantic Current variability through marine isotope stage M2 (circa 3.3 Ma) during the mid-Pliocene. *Paleoceanography*, *24*, PA4206. https://doi.org/10.1029/2008PA001725

De Schepper, S., Head, M. J., & Louwye, S. (2009). Pliocene dinoflagellate cyst stratigraphy, palaeoecology and sequence stratigraphy of the Tunnel-Canal Dock, Belgium. *Geological Magazine*, *146*, 92–112. https://doi.org/10.1017/S0016756808005438

De Schepper, S., Schreck, M., Beck, K., & Matthiessen, J. (2015). Early Pliocene onset of modern Nordic Seas circulation due to ocean gateway changes. *Nature Communications*, *6*, 8659–8658. https://doi.org/10.1038/ncomms9659

de Vernal, A., & Mudie, P. J. (1989a). Late Pliocene to Holocene palynostratigraphy at ODP Site 645, Baffin Bay. In *Proceedings of the Ocean Drilling Program, Scientific Results* (Vol. 105, pp. 387–399). College Station, TX: Ocean Drilling Program.

de Vernal, A., & Mudie, P. J. (1989b). Pliocene and Pleistocene palynostratigraphy at ODP Sites 646 and 647, eastern and southern Labrador Sea. In *Proceedings of the Ocean Drilling Program, Scientific Results* (Vol. 105, pp. 401–422). College Station, TX: Ocean Drilling Program.

Diekmann, M. (1994). Deciduous forest vegetation in Boreo-nemoral Scandinavia. *Acta Phytogeography Suecica*, *80*, 1–112.

Dowsett, H., Dolan, A., Rowley, D., Pound, M., Salzmann, U., Robinson, M., … Haywood, A. (2016). The PRISM4 (mid-Piacenzian) palaeoenvironmental reconstruction. *Climate of the Past*, *12*(7), 1519–1538. https://doi.org/10.5194/cp-12-1519-2016

Dowsett, H. J., Foley, K. M., Stoll, D. K., Chandler, M. A., Sohl, L. E., Bentsen, M., … Zhang, Z. (2013). Sea surface temperature of the mid-Piacenzian Ocean: A data-model comparison. *Scientific Reports*, *3*(1), 1–8. https://doi.org/10.1038/srep02013

Dowsett, H. J., Robinson, M. M., Stoll, D. K., Foley, K. M., Johnson, A. L. A., Williams, M., & Riesselman, C. R. (2013). The PRISM (Pliocene palaeoclimate) reconstruction: Time for a paradigm shift. *Philosophical Transactions. Series A, Mathematical, Physical, and Engineering Sciences*, *371*(2001). 20120524. https://doi.org/10.1098/rsta.2012.0524

Grøsfjeld, K., Harland, R., & Howe, J. (2009). Dinoflagellate cyst assemblages inshore and offshore Svalbard reflecting their modern hydrography and climate. *Norwegian Journal of Geology*, *89*, 121–134.

Haug, G. H., Ganopolski, A., Sigman, D. M., Rosell-Mele, A., Swann, G. E. A., Tiedemann, R., … Eglinton, G. (2005). North Pacific seasonality and the glaciation of North America 2.7 million years ago. *Nature*, *433*, 821–825. https://doi.org/10.1038/nature03332

Haug, G. H., Tiedemann, R., Zahn, R., & Ravelo, A. C. (2001). Role of Panama uplift on oceanic freshwater balance. *Geology*, *29*(3), 207–210. https://doi.org/10.1130/0091-7613(2001)029%3C0207:ROPUOO%3E2.0.CO;2

Haywood, A. M., Dolan, A. M., Pickering, S. J., Dowsett, H. J., McClymont, E. L., Prescott, C. L., … Lunt, D. J. (2013). On the identification of a Pliocene time slice for data–model comparison. *Philosophical Transactions of the Royal Society A - Mathematical Physical and Engineering Sciences*, *371*(2001), 1–21.

Haywood, A. M., Dowsett, H. J., & Dolan, A. M. (2016). Integrating geological archives and climate models for the mid-Pliocene warm period. *Nature Communications*, *7*(May 2015), 10646. https://doi.org/10.1038/ncomms10646

Haywood, A. M., Hill, D. J., Dolan, A. M., Otto-Bliesner, B. L., Bragg, F., Chan, W. L., … Zhang, Z. (2013). Large-scale features of Pliocene climate: Results from the Pliocene model Intercomparison project. *Climate of the Past*, *9*(1), 191–209. https://doi.org/10.5194/cp-9-191-2013

Head, M. J. (1994). Morphology and paleoenvironmental significance of the Cenozoic dinoflagellate genera Tectatodinium and Habibacysta. *Micropaleontology*, *40*(4), 289–321. https://doi.org/10.2307/1485937

Head, M. J. (1996). Late Cenozoic dinoflagellates from the Royal Society borehole at Ludham, Norfolk, eastern England. *Journal of Paleontology*, *70*(04), 543–570. https://doi.org/10.1017/S0022336000023532

Head, M. J. (1998). Pollen and dinoflagellates from the Red Crag at Walton-on-the-Naze, Essex: Evidence for a mild climatic phase during the early Late Pliocene of eastern England. *Geological Magazine*, *135*(6), 803–817. https://doi.org/10.1017/S0016756898001745

Head, M. J., Norris, G., & Mudie, P. J. (1989). New species of dinocysts and a new species of acritarch from the Upper Miocene and lowermost Pliocene, ODP Leg 105, Site 646, Labrador Sea. *Proceedings of the Ocean Drilling Program, Scientific Results*, *105*, 453–466. https://doi.org/10.2973/odp.proc.sr.105.136.1989

Hennissen, J. A. I., Head, M. J., De Schepper, S., & Groeneveld, J. (2014). Palynological evidence for a southward shift of the North Atlantic current at ~2.6 Ma during the intensification of late Cenozoic Northern Hemisphere glaciation. *Paleoceanography*, *29*, 564–580. https://doi.org/10.1002/2013PA002543

Hennissen, J. A. I., Head, M. J., De Schepper, S., & Groeneveld, J. (2017). Dinoflagellate cyst paleoecology during the Pliocene–Pleistocene climatic transition in the North Atlantic. *Palaeogeography Palaeoclimatology Palaeoecology*, *470*, 81–108. https://doi.org/10.1016/j.palaeo.2016.12.023

Herbert, T. D., Lawrence, K. T., Tzanova, A., Peterson, L. C., Caballero-Gill, R., & Kelly, C. S. (2016). Late Miocene global cooling and the rise of modern ecosystems. *Nature Geoscience*, *9*(11), 843–847. https://doi.org/10.1038/ngeo2813

Hilgen, F. J., Lourens, L. J., & Van Dam, J. A. (2012). Chapter 29—The Neogene period. In *The Geologic Time Scale*, (pp. 923–978). Burlington, MA, USA: Elsevier. https://doi.org/10.1016/B978-0-444-59425-9.00029-9

Hill, D. J. (2015). The non-analogue nature of Pliocene temperature gradients. *Earth and Planetary Science Letters*, *425*, 232–241. https://doi.org/10.1016/j.epsl.2015.05.044

Intergovernmental Panel on Climate Change (2013). Climate change 2013: The physical science basis. In T. F. Stocker, et al. (Eds.), *Contribution of Working Group I to the Fifths Assessment Report of the Intergovernmental Panel on Climate Change* (1535 pp.). Cambridge, UK and New York, Cambridge University Press.

Jansen, E., Fronval, T., Rack, F., & Channell, J. E. T. (2000). Pliocene-Pleistocene ice rafting history and cyclicity in the Nordic seas during the last 3.5 Myr. *Paleoceanography*, *15*(6), 709–721. https://doi.org/10.1029/1999PA000435

Jansen, E., & Sjøholm, J. (1991). Reconstruction of glaciation over the past 6 Myr from ice-borne deposits in the Norwegian Sea. *Letter to Natural*, *349*(6310), 600–603. https://doi.org/10.1038/349600a0

Jansson, I. M., Mertens, K. N., Head, M. J., de Vernal, A., Londeix, L., Marret, F., … Sangiorgi, F. (2014). Statistically assessing the correlation between salinity and morphology in cysts produced by the dinoflagellate *Protoceratium reticulatum* from surface sediments of the North Atlantic Ocean, Mediterranean-Marmara-Black Sea region, and Baltic-Kattegat-Skage. *Palaeogeography Palaeoclimatology Palaeoecology*, *399*, 202–213. https://doi.org/10.1016/j.palaeo.2014.01.012

Knies, J., Cabedo-Sanz, P., Belt, S. T., Baranwal, S., Fietz, S., & Rosell-Melé, A. (2014). The emergence of modern sea ice cover in the Arctic Ocean. *Nature Communications*, *5*, 5608. https://doi.org/10.1038/ncomms6608

Knies, J., Mattingsdal R., Fabian K., Grøsfjeld K., Baranwal S., Husum K., … Gaina C. (2014). Effect of early Pliocene uplift on late Pliocene cooling in the Arctic–Atlantic gateway. *Earth and Planetary Science Letters*, *387*, 132–144. https://doi.org/10.1016/j.epsl.2013.11.007

Laskar, J., Robutel, P., Joutel, F., Gastineau, M., Correia, A. C. M., & Levrard, B. (2004). A long-term numerical solution for the insolation quantities of the Earth. *Astronomy and Astrophysics*, *428*(1), 261–285. https://doi.org/10.1051/0004-6361:20041335

Lisiecki, L. E., & Raymo, M. E. (2005). A Pliocene-Pleistocene stack of 57 globally distributed benthic $\delta^{18}O$ records. *Paleoceanography*, *20*, PA1003. https://doi.org/10.1029/2004PA001071

Martínez-Botí, M. A., Foster, G. L., Chalk, T. B., Rohling, E. J., Sexton, P. F., Lunt, D. J., … Schmidt, D. N. (2015). Plio-Pleistocene climate sensitivity evaluated using high-resolution CO_2 records. *Nature*, *518*(7537), 49–54. https://doi.org/10.1038/nature14145

Matthiessen, J. (1995). Distribution patterns of dinoflagellate cysts and other organic-walled microfossils in recent Norwegian-Greenland Sea sediments. *Marine Micropaleontology*, *24*(3-4), 307–334. https://doi.org/10.1016/0377-8398(94)00016-G

McClymont, E., Dekens, P., Dowsett, H. J., Dupont, L. M., Haywood, A. M., & Salzmann, U. (2015). Pliocene climate variability over glacial-interglacial timescales (PlioVAR) working group. *PAGES Magazine*, *23*(2), 2015.

Mertens, K. N., Bringué, M., van Nieuwenhove, N., Takano, Y., Pospelova, V., Rochon, A., … Matsuoka, K. (2012). Process length variation of the cyst of the dinoflagellate *Protoceratium reticulatum* in the North Pacific and Baltic-Skagerrak region: Calibration as an annual density proxy and first evidence of pseudo-cryptic speciation. *Journal of Quaternary Science*, *27*(7), 734–744. https://doi.org/10.1002/jqs.2564

Mertens, K. N., Dale, B., Ellegaard, M., Jansson, I., & Godhe, A. (2010). Process length variation in cysts of the dinoflagellate *Protoceratium reticulatum*, from surface sediments of the Baltic–Kattegat–Skagerrak estuarine system: A regional salinity proxy. *Boreas*, *40*(2), 242–255. https://doi.org/10.1111/j.1502-3885.2010.00193.x

Mertens, K. N., González, C., Delusina, I., & Louwye, S. (2009). 30 000 years of productivity and salinity variations in the late Quaternary Cariaco Basin revealed by dinoflagellate cysts. *Boreas*, *38*(4), 647–662. https://doi.org/10.1111/j.1502-3885.2009.00095.x

Moen, A. (1987). The regional vegetation of Norway; that of central Norway in particular. *Norsk Geologisk Tidsskrift*, *41*(4), 179–226. https://doi.org/10.1080/00291958708552180

Moen, A. (1999). *National Atlas of Norway: Vegetation*. Hønefoss, Norway: Norwegian Mapping Authority.

Mudelsee, M., & Raymo, M. E. (2005). Slow dynamics of the Northern Hemisphere glaciation. *Paleoceanography*, *20*, PA4022. https://doi.org/10.1029/2005PA001153

Naafs, B. D. A., Stein, R., Hefter, J., Khélifi, N., De Schepper, S., & Haug, G. H. (2010). Late Pliocene changes in the North Atlantic Current. *Earth and Planetary Science Letters*, *298*(3-4), 434–442. https://doi.org/10.1016/j.epsl.2010.08.023

Nilsen, J. E. Ø., & Nilsen, F. (2007). The Atlantic Water flow along the Vøring Plateau: Detecting frontal structures in oceanic station time series. *Deep Sea Research Part I: Oceanographic Research Papers*, *54*(3), 297–319. https://doi.org/10.1016/j.dsr.2006.12.012

Otto-Bliesner, B. L., Jahn, A., Feng, R., Brady, E. C., Hu, A., & Löfverström, M. (2017). Amplified North Atlantic warming in the late Pliocene by changes in Arctic gateways. *Geophysical Research Letters*, *44*, 957–964. https://doi.org/10.1002/2016GL071805

Paez-Reyes, M., & Head, M. J. (2013). The Cenozoic Gonyaulacacean Dinoflagellate genera Operculodinium Wall, 1967 and Protoceratium Bergh, 1881 and their phylogenetic relationships. *Journal of Paleontology*, *87*(05), 786–803. https://doi.org/10.1666/12-103

Panitz, S., Salzmann, U., Risebrobakken, B., De Schepper, S., & Pound, M. J. (2016). Climate variability and long-term expansion of peatlands in Arctic Norway during the late Pliocene (ODP Site 642, Norwegian Sea). *Climate of the Past*, *11*(6), 5755–5798. https://doi.org/10.5194/cpd-11-5755-2015

Ravelo, A. C., & Andreasen, D. H. (2000). Enhanced circulation during a warm period. *Geophysical Research Letters*, *27*(7), 1001–1004. https://doi.org/10.1029/1999GL007000

Raymo, M. E., Grant, B., Horowitz, M., & Rau, G. H. (1996). Mid-Pliocene warmth: Stronger greenhouse and stronger conveyor. *Marine Micropaleontology*, *27*(1-4), 313–326. https://doi.org/10.1016/0377-8398(95)00048-8

Reid, P. C. (1977). Peridiniacean and glenodiniacean dinoflagellate cysts from the British Isles. *Nova Hedwigia*, *29*, 429–463.

Risebrobakken, B., Andersson, C., De Schepper, S., & McClymont, E. L. (2016). Low frequency Pliocene climate variability on the eastern Nordic Seas. *Paleoceanography*, *31*, 1154–1175. https://doi.org/10.1002/2015PA002918

Robinson, M. M. (2009). New quantitative evidence of extreme warmth in the Pliocene Arctic. *Stratigraphy*, *6*(4), 265–275.

Rochon, A., de Vernal, A., Turon, J.-L., Matthiessen, J., & Head, M. J. (1999). Distribution of recent dinoflagellate cysts in surface sediments from the North Atlantic Ocean and adjacent seas in relation to sea-surface parameters. *American Association of Stratigraphic Palynologists*, *24*(3-4), 307–334. https://doi.org/10.1016/0377-8398(94)00016-G

Salzmann, U., Dolan, A. M., Haywood, A. M., Chan, W. L., Voss, J., Hill, D. J., … Zhang, Z. (2013). Challenges in quantifying Pliocene terrestrial warming revealed by data-model discord. *Nature Climate Change*, *3*(11), 969–974. https://doi.org/10.1038/nclimate2008

Sarnthein, M., Bartoli, G., Prange, M., Schmittner, A., Schneider, B., Weinelt, M., … Garbe-Schönberg, D. (2009). Mid-Pliocene shifts in ocean overturning circulation and the onset of Quaternary-style climates. *Climate of the Past*, *5*(2), 269–283. https://doi.org/10.5194/cp-5-269-2009

Schreck, M., Meheust, M., Stein, R., & Matthiessen, J. (2013). Response of marine palynomorphs to Neogene climate cooling in the Iceland Sea (ODP Hole 907A). *Marine Micropaleontology*, *101*, 49–67. https://doi.org/10.1016/j.marmicro.2013.03.003

Schreck, M., Seung-Il, N., Clotten, C., Fahl, K., De Schepper, S., Forwick, M., & Matthiessen, J. (2017). Neogene dinoflagellate cysts and acritarchs from the high northern latitudes and their relation to sea surface temperature. *Marine Micropaleontology*, *136*, 51–65. https://doi.org/10.1016/j.marmicro.2017.09.003

Seki, O., Foster, G. L., Schmidt, D. N., Mackensen, A., Kawamura, K., & Pancost, R. D. (2010). Alkenone and boron-based Pliocene pCO_2 records. *Earth and Planetary Science Letters*, *292*(1-2), 201–211. https://doi.org/10.1016/j.epsl.2010.01.037

Shipboard Scientific Party (1987). In O. Eldholm, J. Thiede, & E. Taylor (Eds.), *4. Site 642: Norwegian Sea*, *Init. Repts* (Vol. 104, pp. 53–453). College Station, TX: Ocean Drilling Program.

Skogen, M. D., Budgell, W. P., & Rey, F. (2007). Interannual variability in Nordic seas primary production. *ICES Journal of Marine Science*, *64*(5), 889–898. https://doi.org/10.1093/icesjms/fsm063

Stockmarr, J. (1971). Tablets with spores used in absolute pollen analysis. *Pollen et Spores*, *13*, 615–621.

Swift, J. H. (1986). The Arctic Waters. In B. G. Hurdle (Ed.), *The Nordic Seas* (pp. 129–154). New York: Springer. https://doi.org/10.1007/978-1-4615-8035-5_5

Thorsen, T. A., & Dale, B. (1997). Dinoflagellate cysts as indicators of pollution and past climate in a Norwegian fjord. *Holocene*, *7*(4), 433–446. https://doi.org/10.1177/095968369700700406

Verleye, T. J., Mertens, K. N., Louwye, S., & Arz, H. W. (2009). Holocene salinity changes in the southwestern Black Sea: A reconstruction based on dinoflagellate cysts. *Palynology*, *33*(1), 77–100. https://doi.org/10.2113/gspalynol.33.1.77

Wall, D., & Dale, B. (1966). "Living fossils" in western Atlantic plankton. *Nature*, *211*, 1025–1026. https://doi.org/10.1038/211676a0

Wall, D., Dale, B., Lohmann, G. P., & Smith, W. K. (1977). The environmental and climatic distribution of dinoflagellate cysts in modern marine sediments from regions in the North and South Atlantic Oceans and adjacent seas. *Marine Micropaleontology*, *2*, 121–200. https://doi.org/10.1016/0377-8398(77)90008-1

Williams, G. L., Fensome, R. A., & MacRae, R. A. (2017). The Lentin and Williams index of fossil dinoflagellates 2017 edition. In *Am. Assoc. Stratigr. Palynol. Contrib. Ser. no. 48* (1097 pp).

Zhang, Z. S., Nisancioglu, K. H., Chandler, M. A., Haywood, A. M., Otto-Bliesner, B. L., Ramstein, G., … Ueda, H. (2013). Mid-Pliocene Atlantic Meridional Overturning Circulation not unlike modern. *Climate of the Past*, *9*(4), 1495–1504. https://doi.org/10.5194/cp-9-1495-2013

Zhang, Z. S., Nisancioglu, K. H., & Ninnemann, U. S. (2013). Increased ventilation of Antarctic deep water during the warm mid-Pliocene. *Nature Communications*, *4*, 1499. https://doi.org/10.1038/ncomms2521

Zonneveld, K. A. F., Marret, F., Versteegh, G. J. M., Bogus, K., Bonnet, S., Bouimetarhan, I., … Young, M. (2013). Atlas of modern dinoflagellate cyst distribution based on 2405 data points. *Review of Palaeobotany and Palynology*, *191*, 1–197. https://doi.org/10.1016/j.revpalbo.2012.08.003